A NAVIER-STOKES CALCULATION OF THE FLOW PASSING THROUGH A CASCADE WITH TIP CLEARANCE

ICAS-90-4.2.3

Toshinori Watanabe
Tokyo University of Agriculture and Technology
2-24-16 Nakamachi, Koganei, Tokyo, 183, Japan

Osamu Nozaki and **Atsuhiro Tamura**
National Aerospace Laboratory
7-44-1, Jindaiji-Higashi, Chofu, Tokyo, 182, Japan

Abstract

The three-dimensional viscous flow fields through cascades with tip clearance were numerically studied by solving the Navier-Stokes equations. LU-ADI scheme was used for the calculation. The computational grid was generated by a zonal method. A fundamental cascade composed of flat plates, on which corresponding experimental data were available, was adopted to develop the appropriate solution method for the flow through the tip clearance. The computed results showed good agreement with the experimental data and the reliability of the developed method was verified. The detailed flow phenomena around the blade tip, such as the formation of separation bubbles on the tip surface, were clearly described. It was found that the normal force acting on the extremity of the blade did not diminish in the case of small clearances. The flow field in a linear turbine cascade was simulated by the method next and the results also showed good agreement with the experimental data. It was realized that the influence of wall boundary layers should be taken into consideration in the inlet flow condition for computation. The method was further applied to a rotating fan and the complicated flow field near the blade tip was clearly shown on the rotating frame of reference.

Nomenclature

C_N	:normal force coefficient
I	:rothalpy
J	:Jacobian
Pr	:Prandtl number
V_θ	:rotational component of velocity
a	:speed of sound
c	:local coordinate on the blade chord
c_0	:chord length
e	:energy
h_0	:span length between hub and tip walls
j,k,l	:numbers of grid points
p	:static pressure
t	:time
u,v,w	:velocity components in x, y and z directions, respectively
x,y,z	:Cartesian coordinates
α	:angle of attack
β	:inlet flow angle
γ	:ratio of specific heats
δ	:tip clearance
ξ, η, ζ	:general curvilinear coordinates
μ	:viscosity coefficient
ρ	:density
ω	:angular velocity of rotation

1. Introduction

In the cascades of turbomachines, there are tip clearances between blade tips and casing walls. The tip leakage flow and the tip vortex owing to the tip clearance have considerable influences on the three-dimensional flow fields around cascades. Moreover, the flow through tip clearance is profoundly connected with the loss generation. Therefore, the understanding of the detailed flow field near the blade tip including the effect of tip clearance is one of the most important matters for the present turbomachinery.

Since the flow field in the tip region is governed by the viscous property of the fluid, the analytical studies based on the potential theory is not effective for the practical purpose mentioned above.

In this study, the three-dimensional viscous flow through cascades with tip clearance were numerically investigated by solving the Navier-Stokes equations. The assumption of the thin-layer approximation was adopted to reduce the computational load. LU-ADI factorization method[1] was used as the numerical algorithm. The computational grid was generated by a zonal method with an overlapping grid technique.[2] The computational method for the cases without tip clearance was previously presented[3] and it was improved in this study for the flow through the tip clearance.

A fundamental linear cascade composed of flat plates, on which corresponding experimental data were available, was dealt with first in order to establish the appropriate solution method. The calculated results were compared with the experimental data and the effectiveness of the developed code was discussed.

Further, the developed method was applied to a linear turbine cascade and a rotating fan. The characteristics of the complicated flow in tip regions were studied based on the computational results.

2. Computational Method

2.1 Governing Equations and Numerical Algorithm

The equations of continuity, momentum and energy are written on the rotating coordinate system attached to rotor blades and transformed to the general coordinate system (ξ, η, ζ).

These equations are expressed in the conservation-law form as follows:

$$\frac{\partial \hat{Q}}{\partial t}+\frac{\partial \hat{E}}{\partial \xi}+\frac{\partial \hat{F}}{\partial \eta}+\frac{\partial \hat{G}}{\partial \zeta}=\frac{1}{Re}\left[\frac{\partial \hat{S}_1}{\partial \eta}+\frac{\partial \hat{S}_2}{\partial \zeta}\right]+\hat{T} \quad (1)$$

where

$$\hat{Q}=\frac{1}{J}\begin{bmatrix}\rho\\ \rho u\\ \rho v\\ \rho w\\ \rho I-P\end{bmatrix} \qquad \hat{E}=\frac{1}{J}\begin{bmatrix}\rho U\\ \rho uU+\xi_x P\\ \rho vU+\xi_y P\\ \rho wU+\xi_z P\\ \rho IU\end{bmatrix}$$

$$\hat{F}=\frac{1}{J}\begin{bmatrix}\rho V\\ \rho uV+\eta_x P\\ \rho vV+\eta_y P\\ \rho wV+\eta_z P\\ \rho IV\end{bmatrix} \qquad \hat{G}=\frac{1}{J}\begin{bmatrix}\rho W\\ \rho uW+\zeta_x P\\ \rho vW+\zeta_y P\\ \rho wW+\zeta_z P\\ \rho IW\end{bmatrix}$$

$$\hat{T}=\frac{1}{J}\begin{bmatrix}0\\ 0\\ \rho\omega(\omega y+2w)\\ \rho\omega(\omega z-2v)\\ 0\end{bmatrix}$$

$$U=\xi_x u+\xi_y v+\xi_z w$$
$$V=\eta_x u+\eta_y v+\eta_z w$$
$$W=\zeta_x u+\zeta_y v+\zeta_z w$$

$$I=\frac{(e+P-r\omega V_\theta)}{\rho}$$

$$\hat{S}_1=\frac{1}{J}\begin{bmatrix}0\\ \mu m_1 u_\eta+(\mu/3)m_2\eta_x\\ \mu m_1 v_\eta+(\mu/3)m_2\eta_y\\ \mu m_1 w_\eta+(\mu/3)m_2\eta_z\\ \mu m_1 m_3+(\mu/3)m_2(\eta_x u+\eta_y v+\eta_z w)\end{bmatrix}$$

$$m_1=\eta_x^2+\eta_y^2+\eta_z^2$$
$$m_2=\eta_x u_\eta+\eta_y v_\eta+\eta_z w_\eta$$

$$m_3=\frac{1}{2}(u^2+v^2+w^2)+\frac{1}{Pr(\gamma-1)}\frac{\partial a^2}{\partial \eta}$$

$$\hat{S}_2=\frac{1}{J}\begin{bmatrix}0\\ \mu n_1 u_\zeta+(\mu/3)n_2\zeta_x\\ \mu n_1 v_\zeta+(\mu/3)n_2\zeta_y\\ \mu n_1 w_\zeta+(\mu/3)n_2\zeta_z\\ \mu n_1 n_3+(\mu/3)n_2(\zeta_x u+\zeta_y v+\zeta_z w)\end{bmatrix}$$

$$n_1=\zeta_x^2+\zeta_y^2+\zeta_z^2$$
$$n_2=\zeta_x u_\zeta+\zeta_y v_\zeta+\zeta_z w_\zeta$$

$$n_3=\frac{1}{2}(u^2+v^2+w^2)+\frac{1}{Pr(\gamma-1)}\frac{\partial a^2}{\partial \zeta}$$

In the Navier-Stokes equations shown above, the thin layer approximation is used. In the cases of stationary cascades, the terms related to the rotation, that is, $\hat{T}$ and V_θ, are removed.

Equation (1) is solved by the LU-ADI factorization scheme, the details of which are given in reference 1.

In this study, flow fields were assumed to be laminar.

2.2 Computational Grid and Boundary Conditions

Figure 1 shows the schematic diagram of the typical computational grid. In Fig.1, the C-type grid on the hub wall is shown. C-type grids are stacked in the spanwise direction from the hub side wall to the tip side wall in order to generate the three-dimensional grid. The region between the tip surface of the blade and the tip wall is filled with H-type grid as shown in Fig.2. By this method, the flat tip surface and its sharp edge can be accurately represented. C-type and H-type grids are overlapped at their interface for the smooth connection of computed values. Overlapping grids are also used on the periodic boundary. Communication on the overlapped boundaries is achieved by means of the linear interpolation along the grid lines.

At the upstream boundary, which is 1.7 times of the chord length upstream from the leading edge, the total pressure and the total temperature are held constant and the inlet flow angle is prescribed. The other variables are extrapolated. At the downstream boundary, which is 2.5 times of the chord length downstream from the trailing edge, the static pressure is specified. On the blade surfaces and the walls, non-slip and adiabatic conditions are used. A permeable condition is used at the wake boundary.

3. Cascade Models for Calculation

Three types of cascades were used for the calculation. They were: 1) a linear stationary cascade composed of flat plates, 2) a stationary turbine cascade, and 3) a rotating fan in an annular duct. Corresponding experimental results were available for 1) and 2) cascades.

1) is the fundamental model used for the establishment of the computational method for the cascades with tip clearance. It is schematically shown in Fig.1. The aerodynamic characteristics of this cascade were studied experimentally by one of the authors.[4] Each blade has a chord length of 60mm and a thickness of 6mm. Their leading and trailing edges are shaped into semicircles in cross section. The blade span is 180mm including the tip clearance. The clearance is changed up to 5mm.

2) is a more realistic case than 1) on which the detailed flow measurement, including the flow in the tip clearance, was performed by Yamamoto.[5] The computational grid is shown in Fig.3. The solidity of the cascade is 1.20 (the chord

length of each blade is 73.5mm), the aspect ratio is 1.37 and the tip clearance is 2.7% of the blade span. The turning angle is 107.1 degrees.

3) is a realistic high-bypass fan designed in National Aerospace Laboratory Japan. It is composed of 16 strongly twisted blades as shown in Fig.4. The chord length at the midspan is 42.7mm. The outer radius of the fan duct is 225.0mm and the inner one is 112.5mm.

4. Results and Discussions

4.1 Linear Cascade

The case of a linear cascade was calculated first. Figure 1 and figure 2 represent computational grids for the cascade. The number of C-type grid points is 181*65*31 in ξ, η and ζ directions respectively and that of H-type grid points is 62*26*25. The inlet Mach number is about 0.5, though the corresponding Mach number in the experiment was about 0.1.

Figure 5 shows the normal force coefficient C_N against the inlet flow angle β. The computed results are compared with experimental results in this figure and show good agreement. Because the blade load is 0 at $\beta = 50°$ in the calculated result, the angle of attack α is determined to be 0° at this angle. The slight difference of zero-lift angle between computed and experimental results is considered to be caused by the difference of Mach number and the assumption of a laminar flow.

The velocity vectors on the plane perpendicular to the mean flow are shown in Fig.6 for the position of 20mm (one third of the blade chord length) downstream from the blade trailing edge. The angle of attack α is 5 degrees (the cascade works as a compressor) and the tip clearance δ is 5mm. Figure 6(a) shows the experimental results measured with 5-hole pitot tube. It can be said that the calculated results (Fig.6(b)) well describe the experimental results.

Beside these, the computational results were compared with experimental results about the trace of the tip vortex, the distribution of the static pressure on blades, and so on. Since all the computed results showed good agreement with experimental results, it can be concluded that the developed method is effective for the qualitative analysis of the flow through cascades with tip clearance.

Then the detailed flow field around a blade tip was visualized from the computed results.

Figure 7 shows the velocity vectors on a plane close to the tip surface of a blade. The plane is parallel to the tip surface. The flow through the tip clearance is seen to separate at the edge between the tip surface and the pressure surface of a blade and reattach to the tip surface. As a result, a separation bubble is formed on the tip surface. Near the leading edge, a region of the reverse flow is found. It is due to the flow separation at the leading edge of the tip surface as will be shown in the next figure.

Figure 8 shows the velocity vectors near the leading edge of the tip surface. In Fig.8, the vectors on the plane including the center line of the blade profile are seen from the pressure side of the blade. The velocity component toward the casing wall emerges near the leading edge of the tip surface. The flow separates at this edge and form a separation bubble on the tip surface.

Figure 9 is the velocity vector diagram of the tip leakage flow. It shows the vectors on the plane perpendicular to the blade chord. The location of the plane is 60% of the chord length from the leading edge. Vectors are viewed from the leading edge side. The angle of attack is 5 degrees and the tip clearance is 5mm. It is clearly found that the leakage flow rolls up into a tip vortex on the suction side of the blade. The generation of a separation bubble on the tip surface is also captured clearly.

As for the case of the small tip clearance of 0.1mm (Fig.10), no remarkable phenomenon is seen, though a small quantity of leakage flow is observed.

Figure 11 shows the computed oil flows on the tip surface for the case of $\alpha = 5°$ and $\delta = 5$mm. The reverse flow region due to the separation bubble on the leading edge can be clearly seen. Another region of the reverse flow is seen in the pressure side. It is owing to the separation bubble formed by the tip leakage flow. The formed separation bubble covers a wide range of the pressure side on the tip surface.

When the tip clearance is small, the circulation around a blade is known not to diminish at the tip. Figure 12 shows the spanwise distribution of the normal force coefficient C_N near the tip. C_N on the tip is about zero when the tip clearance is 1mm. However, when the clearance is under 1mm, C_N on the tip has a finite value, that is, a finite circulation is retained at the tip. The value of C_N on the tip increases with a decrease in the tip clearance.

4.2 Turbine Cascade

The flow field through a linear turbine cascade was numerically analyzed with the developed code. The experimental data are also available for this cascade. Figure 3 shows the computational grid for this cascade. The generation method of the grid is identical to the one used for the linear cascade.

Figure 13 shows the examples of computational and experimental results. The inlet flow angle is 57 degrees (incidence angle is 7.2 degrees). The outlet Mach number is about 0.5, though the value in the experiment was about 0.1. Figure 13(a) is the pressure distribution in the tip clearance region. The pressure contours are drawn on the middle plane between the side wall and the plane which includes tip surfaces. Figure 13(b) shows the velocity vectors on the same plane as

the pressure contours are drawn. The corresponding experimental results are shown in Fig.13(c). It can be said that the calculated results agree well with the experimental results. In this calculation, however, the velocity distribution in the wall boundary layers were given according to the experimental data. In the preliminary calculation, the used inlet condition was constant in the spanwise direction and the results were not sufficient. It thus appears that the influence of the wall boundary layer should be taken into account in the inlet condition for three-dimensional calculations.

4.3 Rotating Fan

For the more realistic calculation than above two cases, the rotating fan was dealt with. The computation was performed on the rotating frame of reference fixed on the rotating cascade where the effect of the centrifugal force and the Coriolis force were taken into consideration.

Figure 4 shows the schematic diagram of the computational grid for the test fan used for the calculation. The grid was generated by the same method as in the above cases.

The computation was performed at the design point where the rotational speed of the cascade was 12,732rpm, the inlet and outlet Mach number was about 0.84 and 0.70, respectively. The adopted tip clearances were 0.5mm, 1.0mm and 2.0mm.

The computed velocity vectors on a plane in the tip clearance region were drawn in Fig.14(a). The tip clearance in this case was 2mm. The plane is at the middle between the outer casing wall and the tip surface. The strong leakage flow is observed in the rear part of the blade. The pressure contours on the same plane are shown in Fig.14(b). A low pressure part is found at the region corresponding to the strong leakage flow shown in Fig.14(a). At the boundary between C-type and H-type grid, calculated pressures are smoothly connected as in Fig.14(b).

Figure 15(a) shows the vorticity contours on the midchord plane perpendicular to the axis of rotation. The tip clearance is 2mm. In the suction side of a blade, a region of high vorticity due to the tip leakage flow is observed. This region is pressed to the outer casing wall because of the centrifugal force. A lump of large vorticity is also observed at the hub corner of the blade suction side, which is due to the corner vortex. Vorticity contours on a downstream plane is indicated in Fig.15(b). The plane is at the position of 0.5 chord length downstream from the blade trailing edge. On the casing wall, the center of the tip vortex is clearly shown in the middle region of a blade-to-blade channel. The tip vortex is pressed against the casing wall by the centrifugal force and deformed to a flat shape. Blade wakes have thick regions with lumped vorticity.

Figure 16 is the velocity vector diagram of the tip leakage flow. Vectors are plotted on the plane perpendicular to the rotational axis at the midchord position. The tip clearance is 1mm. It is found that the leakage flow separates at the pressure side edge of the tip surface and forms a separation bubble on the tip surface. These are the same phenomena as those observed in the case of the stationary linear cascade. In the suction side of the blade, the outward secondary flow owing to the centrifugal force can be seen. On the suction side edge of the tip surface, the outward flow on the suction surface is drawn into the backward flow on the tip surface due to the separation bubble. The flow field around the tip clearance was thus found very complicated particularly in the case of the rotating cascade.

5. Conclusion

Three-dimensional subsonic flows through cascades with tip clearance were analyzed numerically by use of the Navier-Stokes equations. The computational grid was generated by a zonal method in which the C-type grid was generated around a blade and H-type grid was inserted in the space between the blade tip surface and the outer casing wall.

The computation was performed for a linear cascade composed of flat plates, a linear turbine cascade and a rotating fan. Computed results for linear cascades showed good agreement with available experimental data and the detailed flow phenomena in the tip clearance region, such as the separation of the leakage flow at the pressure side edge of the tip surface and the formation of the separation bubble on the tip surface, were clearly expressed. In these calculations, the importance of taking account of the influence of the wall boundary layer on the inlet flow condition was recognized.

From the results for the rotating fan, the detailed flow aspects in the tip region were clarified under the influence of the centrifugal force and Coriolis force. Since no available experimental result exists for this case, the verification of the calculated results should be made in future.

The developed computational method is thought to be useful for the understanding of the detailed flow field in the three-dimensional cascade including the effect of tip clearance.

References

1)Fujii, K. and Obayashi, S.,"Practical Applications of New LU-ADI Scheme for the Three-Dimensional Navier-Stokes Computation of Transonic Viscous Flows," AIAA Paper 86-0513, 1986.
2)Nakahashi, K., Nozaki, O., Kikuchi, K. and Tamura, A.,"Navier-Stokes Computations of Two- and Three-Dimensional Cascade Flow Fields," AIAA Paper 87-1315, 1987.
3)Nozaki, O., Nakahashi, K. and Tamura, A.,"Numerical Analysis of Three Dimensional Cascade Flow by Solving Navier-Stokes Equations," Proceedings of

the 1987 Tokyo International Gas Turbine Congress II, pp.325-331, 1987.
4)Watanabe, T.,"Research on the Aerodynamic Characteristics of an Oscillating Cascade with Tip Clearance," Ph.D. thesis, Dept. of Aeronautics, Univ. of Tokyo, 1986. (In Japanese)
5)Yamamoto, A.,"Interaction Mechanisms Between Tip Leakage Flow and the Passage Vortex in a Linear Turbine Rotor Cascade", Transactions of the ASME, Journal of Turbomachinery, Vol.110, pp.329-338, 1988.

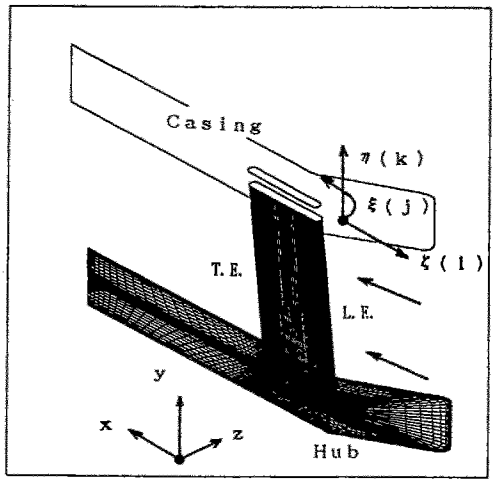

Fig.1 Computational grid for linear cascade

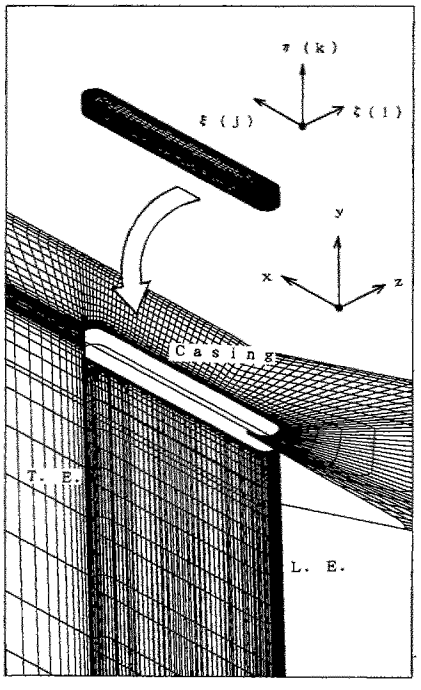

Fig.2 Grid for tip clearance region

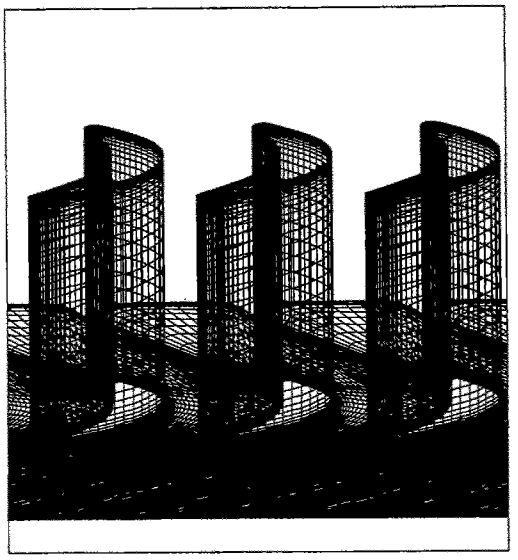

Fig.3 Computational grid for turbine cascade

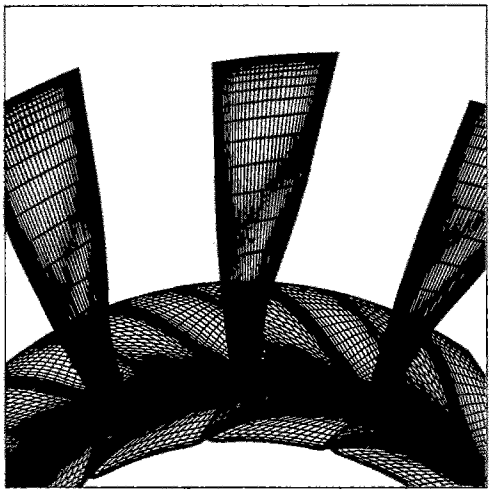

Fig.4 Computational grid for rotating fan

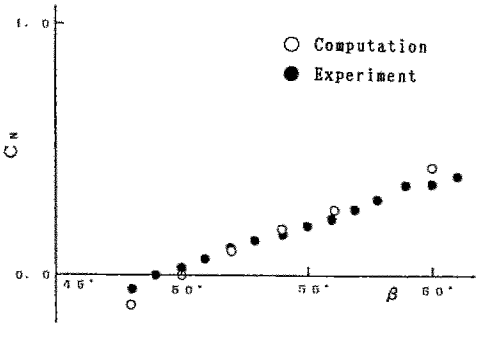

Fig.5 Variation of the normal force at the midspan due to the inlet flow angle

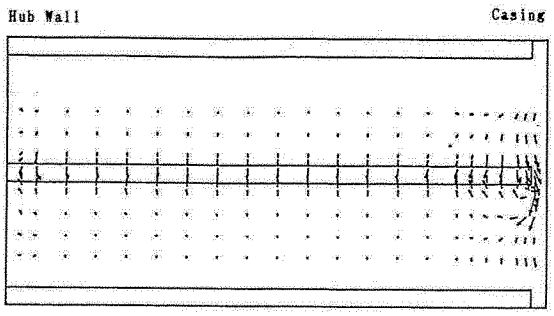

(a) experiment

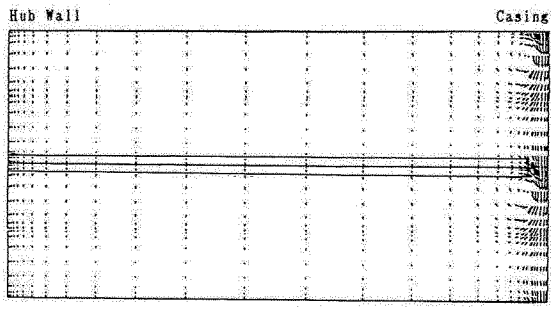

(b) computation

Fig.6 Velocity vectors of the secondary flow at a downstream position
($\alpha = 5°$, δ =5mm, 20mm downstream from the trailing edge)

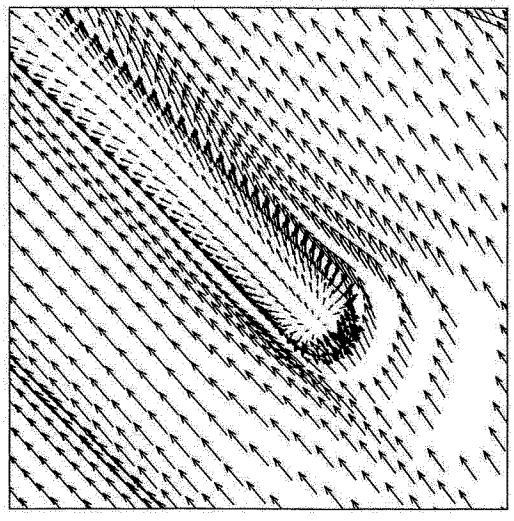

Fig.7 Vector diagram for tip leakage flow
($\alpha = 5°$, δ =5mm, upper right side is the suction side of the blade)

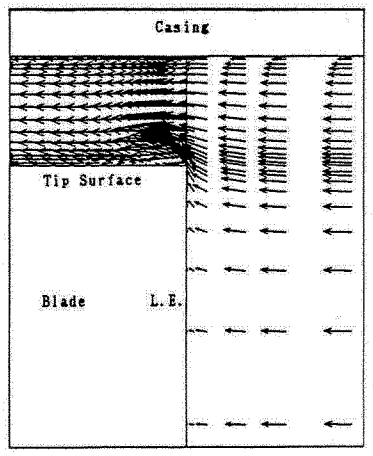

Fig.8 Velocity vectors around the leading edge of the tip surface
($\alpha = 5°$, δ =5mm)

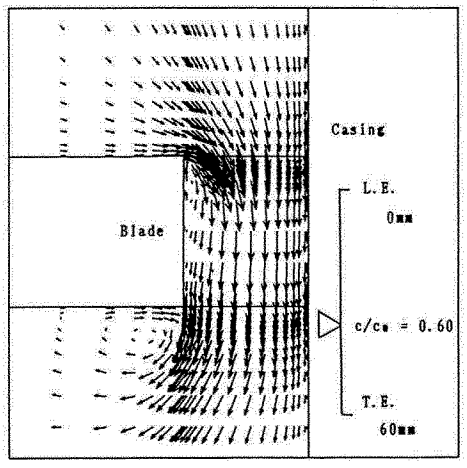

Fig.9 Velocity vectors of the leakage flow (in a plane perpendicular to the blade chord, $\alpha = 5°$, δ =5mm, c/c_0=0.6)

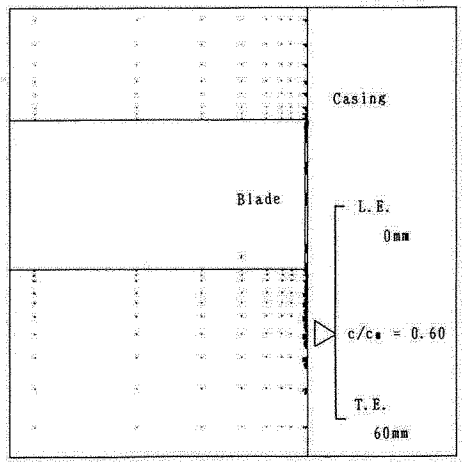

Fig.10 Velocity vectors of the leakage flow
(in a plane perpendicular to the blade chord, $\alpha = 5°$, δ =0.1mm, c/c_0=0.6)

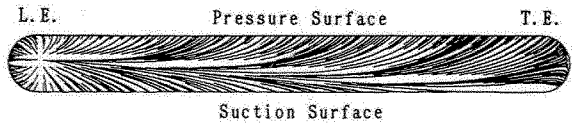

Fig.11 Computed oil flows on the tip surface

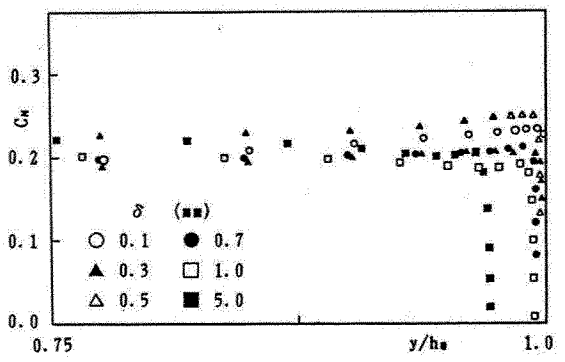

Fig.12 Spanwise distribution of the normal force (near the blade tip)

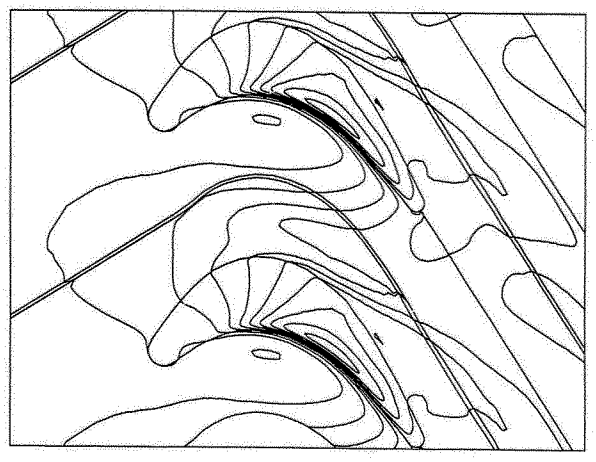

(a) computed pressure contours on the middle plane between the blade tip and the casing

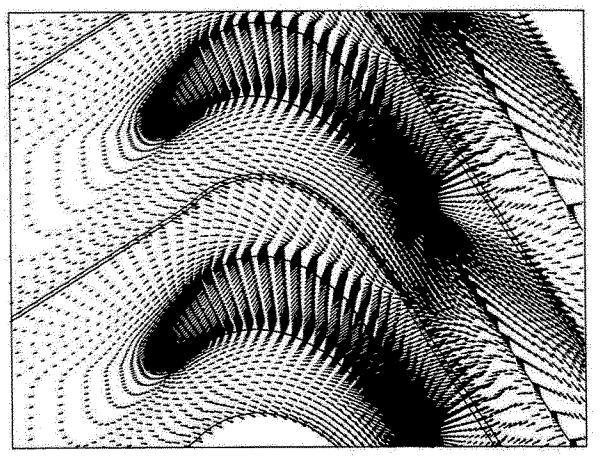

(b) computed velocity vectors

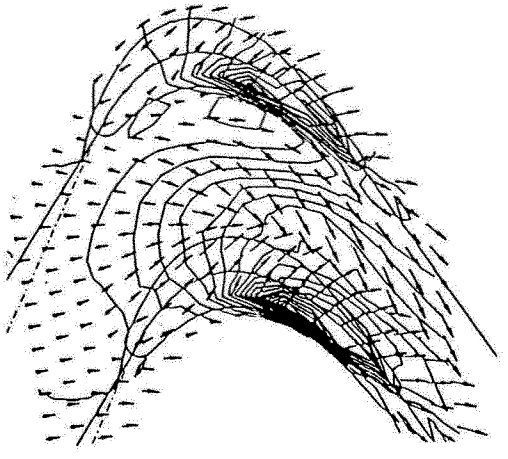

(c) experimental results

Fig.13 Examples of the computational results for turbine cascade (with experimental results, δ=2.7% of the blade span, incidence angle is 7.2°)

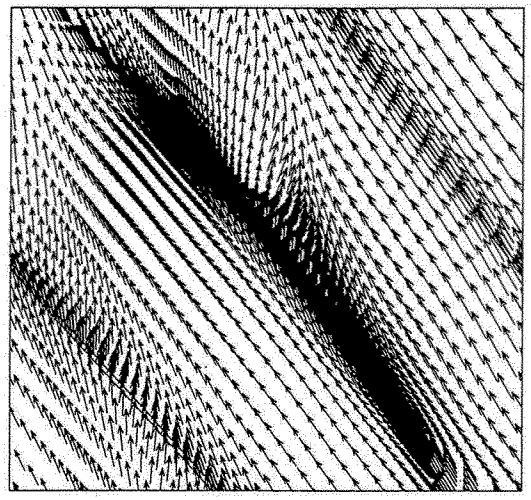

(a) velocity vectors

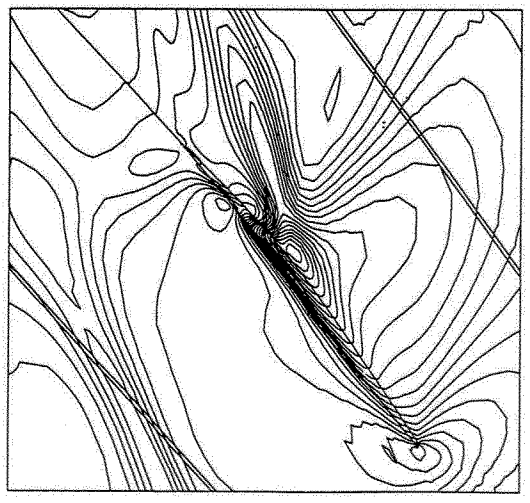

(b) pressure contours

Fig.14 Computational results of the leakage flow for the rotating fan (δ=2mm, results on the middle plane between the blade tip and the casing are shown)

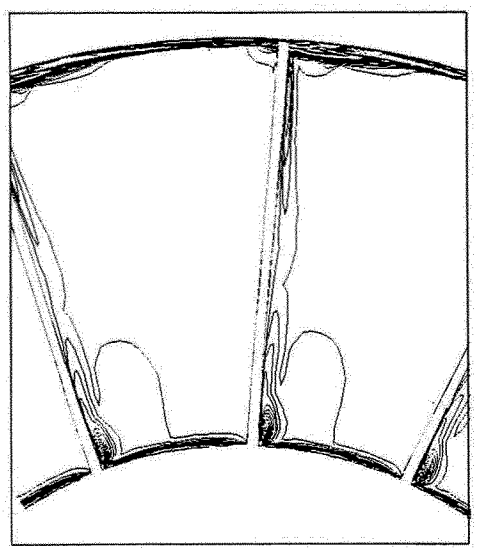

(a) midchord (c/c_0=0.5)

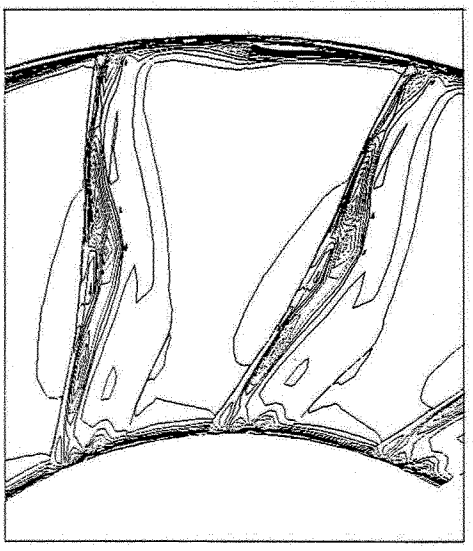

(b) downstream (half of the chord length downstream from the trailing edge)

Fig.15 Vorticity contours on the plane perpendicular to the rotating axis (δ=2mm)

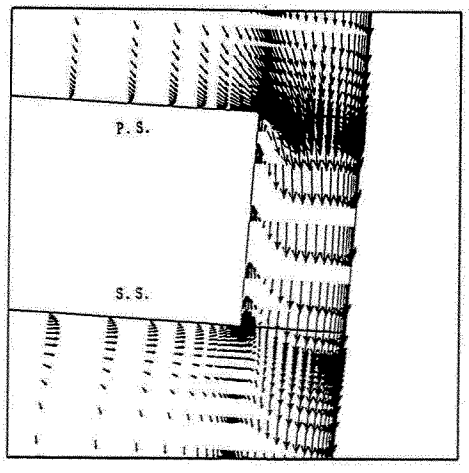

Fig.16 Velocity vectors of the leakage flow
(in a plane perpendicular to the rotating axis, δ=1mm, c/c_0=0.5)